International Society
for Biofabrication

PURPOSE-LED
PUBLISHING™

PAPER • OPEN ACCESS

A compartmentalized microfluidic platform to investigate immune cells cross-talk in rheumatoid arthritis

View the article online for updates and enhancements.

Biofabrication

PAPER

A compartmentalized microfluidic platform to investigate immune cells cross-talk in rheumatoid arthritis

Cecilia Palma[1] , Bianca Aterini[1] , Erika Ferrari[1,2] , Marta Mangione[3] , Martina Romeo[3] ,
Luigi Nezi[3] , Silvia Lopa[4] , Teresa Manzo[5] , Paola Occhetta[1,6,*] and Marco Rasponi[1,6,*]

1   Department of Electronics, Information and Bioengineering, Politecnico di Milano, Via Ponzio 34/5, Milan 20133, Italy
2   BiomimX Srl, Viale Decumano 41, MIND – Milano Innovation District, Milan 20157, Italy
3   Department of Experimental Oncology, European Institute of Oncology IRCCS, Via Adamello 16, Milan 20139, Italy
4   Cell and Tissue Engineering Laboratory, IRCCS Istituto Ortopedico Galeazzi, Via C. Belgioioso 173, Milan 20157, Italy
5   Department of Molecular Biotechnology and Health Sciences, University of Turin, Piazza Nizza 44, Turin 10126, Italy
6   Equally contributing authors.
*   Authors to whom any correspondence should be addressed.

E-mail: paola.occhetta@polimi.it and marco.rasponi@polimi.it

Keywords: rheumatoid arthritis, immune cells, migration, organ-on-chip, microfluidic valves

Supplementary material for this article is available online

Abstract

The dysregulation of the immune system plays a crucial role in the pathogenesis of manyfold diseases, among which we find rheumatoid arthritis (RA), an autoimmune disease characterized by chronic inflammation in synovial joints, leading to pain and disability. Immune cells such as pro-inflammatory macrophages and T helper 1 (Th1) cells drive the inflammatory cascade. Thus, including immune system in *in vitro* models is pivotal to recapitulate and better understand the complex interactions between these immune cell subsets and their secreted mediators. Here, a compartmentalized microfluidic platform is presented, for precise confinement of circulating immune cells in organs-on-chip. The integration of innovative normally-closed sieving valves allows, through minimal waste of biological material, to co-culture different immune cell types (e.g. macrophages and Th1). Moreover, the platform allows to stimulate cell subsets separately, and to assess their cross-talk at desired time points. Functional validation of the platform demonstrates its ability to create stable chemotactic gradients, allowing for induction and evaluation of Th1 cells migration. In a proof-of-concept study, the platform allowed to assess Th1 T cells migration towards pro-inflammatory macrophages, thus replicating a characteristic interaction among immune cells triggered during RA onset. These results thus support the suitability of the platform to study immune cells cross-talk and migration phenomena, being potentially applicable to a manyfold immune cell mechanisms, both involved in RA progression and in different immune-mediated pathologies.

1. Introduction

The immune system plays a pivotal role in maintaining tissue homeostasis and orchestrating immune response during the progression of many diseases, among which rheumatoid arthritis (RA) is a relevant example [1]. RA is a chronic autoimmune disease that involves synovial joints, resulting in disability and reduced life expectancy [2], and its hallmark is an uncontrolled systemic inflammatory response, characterized by immune cells infiltrating in the joints, that first undermine the synovium, causing

inflammation and hyperplasia, and progressively lead to cartilage and bone degradation, with severe joint swelling and pain [3, 4]. RA pathogenesis is intricately linked to dysregulation of the immune system, with a diverse array of immune cells and cytokines that play pivotal roles in orchestrating the inflammatory cascade [5, 6]. In particular, the inflammatory milieu in RA is heavily influenced by the imbalance between pro-inflammatory (M1) and anti-inflammatory (M2) macrophages, which is a crucial driver of RA pathogenesis [7, 8]. Specifically, there is a notable predominance of M1 macrophages in

peripheral blood, synovial fluid and synovium, where M1 macrophages promote inflammation and tissue damage. Moreover, the interplay between these macrophages and CD4+ T helper type 1 (Th1) and T helper type 17 (Th17) cells plays a key role in amplifying the inflammatory processes [9]. On one hand, synovial macrophages produce a combination of pro-inflammatory cytokines, chemokines, and matrix-degrading enzymes [10, 11]. On the other hand, circulating Th1 and Th17 cells are attracted in the joint by such specific macrophage-secreted stimuli and are in turn responsible for the secretion of pro-inflammatory cytokines (such as IFN-γ and TNF-α) that not only drive local inflammation, but also activate other immune cells and stimulate the production of autoantibodies [12]. The interaction between synovial macrophages and Th1/Th17 cells thus leads to a positive feedback loop, worsening the chronic inflammation and tissue damage observed in RA [13]. Despite significant advancements in our understanding of RA, the exact etiology and underlying molecular mechanisms leading to immune dysregulation and joint damage remains not completely elucidated [2]. A better understanding of the complex interactions and early cause-effect relationship between immune cell subsets and their secreted mediators would in turn be crucial for the development of targeted therapeutic strategies, potentially improving patient-specific outcomes and minimizing adverse effects [14, 15].

Traditionally, immune system research has primarily occurred through *in vivo* animal studies or in two-dimensional (2D) traditional *in vitro* cultures. However, in the former case notable disparities exist between immune systems of different animal species, resulting in limited translational efficacy from animal to human trials and contributing to attrition within the drug development process. On the other hand, *in vitro* research using 2D cell cultures falls short in fully mimicking the complexity and the intricate multicellular microenvironment of *in vivo* scenarios [16]. In this context, advanced technologies such as organ-on-chip (OoC) platforms are revolutionizing our ability to study complex immune cellular interactions within physiologically relevant microenvironments [17–19]. In the last decade, several OoC have emerged, integrating immune system components and investigating a wide range of pathophysiological processes, such as immune cell extravasation, immune system interaction with other tissues and organs (e.g. skin, gut, liver), as well as immune responses to tumors and inflammatory processes [16, 20–22]. Microfluidic designs integrating immune cells in OoC may be broadly classified in static versus perfusion-based approaches. Regarding the first type, poly-dimethylsiloxane (PDMS) devices made of three chambers

separated by pass-through trapezoidal posts have been extensively used to assess immune cells chemotaxis through a 3D matrix, in static conditions [23]. Tiberti *et al* exploited a microfluidic device of this kind to evaluate invasion of neutrophils in collagen gel in presence of interstitial fluid derived from colorectal cancer patients [24]. In another study, Pavesi *et al* used a similar device to study the migration of human T cells, engineered to express tumor-specific receptors, in response to human cancer hepatocytes incorporated in a 3D collagen gel [25]. Other designs have been proposed integrating perfusion systems to simulate immune cells circulating together with blood flow. An example is represented by the lung-on-chip model presented from van Os *et al* consisting of a three-channel perfusable system mimicking the lung endothelium, an ECM barrier, and the lung epithelium [26]. The device was exploited to assess the behavior of peripheral blood mononuclear cells (PBMCs) perfused through an endothelium composed of human pulmonary microvascular endothelial cells, in response to inflammation of the epithelial layer. Main drawbacks related to the integration of immune cells in current OoC, either using a static or a perfused configuration, include a poor control over immune cells spatio-temporal location and the need of a considerable amount of immune cells. The precise location of immune cells is an enabling factor for the accurate quantification of their recruitment dynamics [27]. Whereas, despite the microscale dimensions of OoC, the need of large numbers of cell is usually due to two intertwined reasons: (i) an extremely low seeding efficiency (i.e. the number of cells remaining in the channel as compared to the total cells injected), (ii) the high absolute number of cells contained in the initial suspension [28, 29]. This high demand of cells often represents an impairing factor for the application of immune system in *in vitro* models, especially when rare cell populations and/or patient specific models are required.

Here, we report a novel technological solution, which we have termed '*Normally-Closed (NC) Sieving Valves*', conceived to confine immune cells in OoC platforms maximizing seeding procedure efficiency without the need of external pumps, ultimately aiming at applications with rare cell populations, such as T cell subpopulations isolated from patient-derived blood samples. In the perspective of recapitulating a patient-derived RA joint-on-chip model, *NC sieving valves* were integrated in a compartmentalized OoC platform, named here arbitrary 'iMμne', and aimed at evaluating the active interaction of different subsets of immune cells involved in RA. In detail, owing to the incorporation of microfluidic valves, the device allows to host different cell types (i.e. macrophages and Th1 cells) in compartmentalized regions, to stimulate them separately and to

assess their cross-talk by evaluating Th1 migration at specific time points. The platform was technically validated and biologically qualified, in a proof-of-concept study. Specifically, although RA is governed by very complex mechanisms, here we first focused on replicating a simplified process, i.e. the interaction between pro-inflammatory macrophages and activated Th1 cells [30].
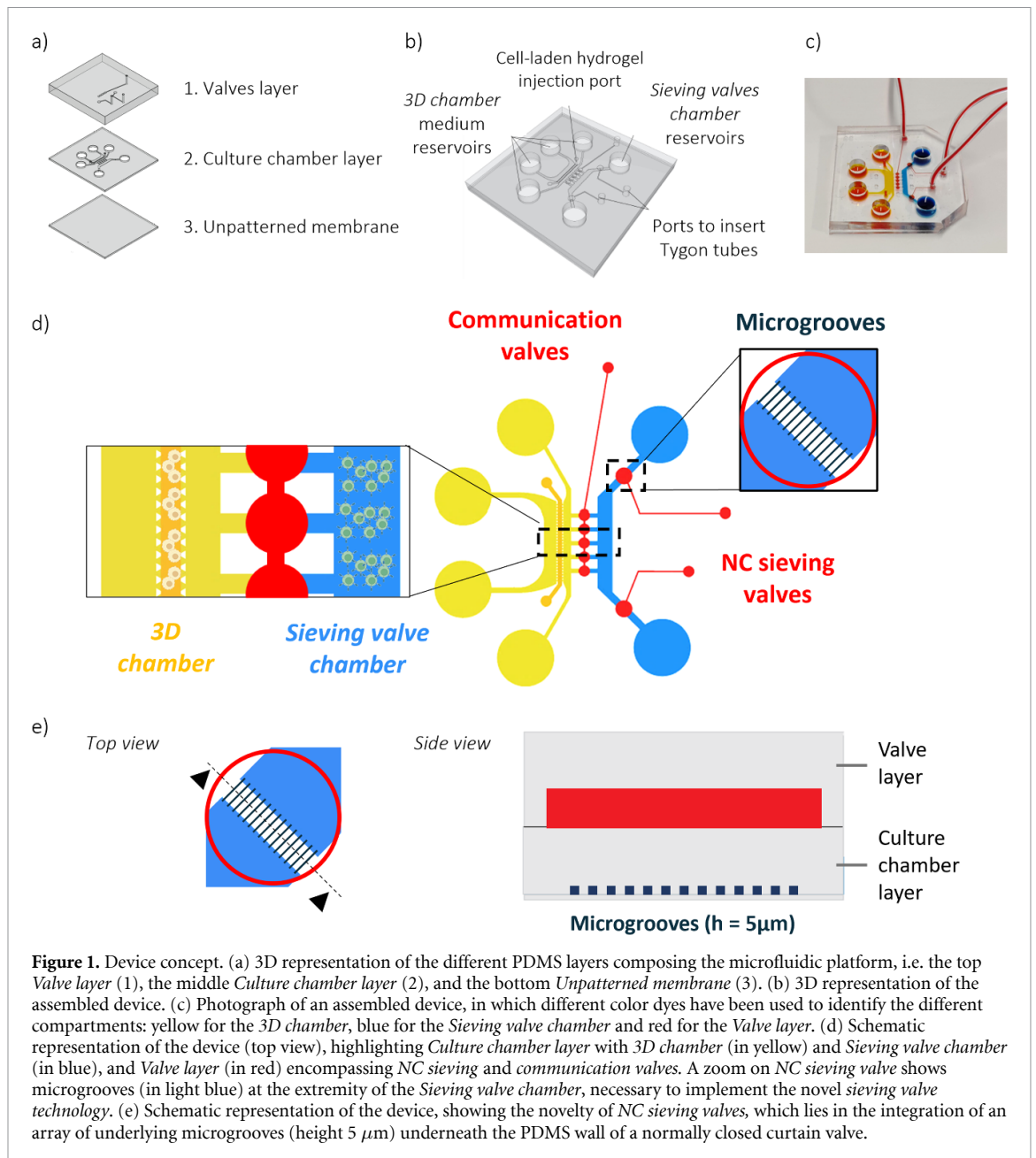
2. Results

2.1. Device concept
A compartmentalized valve-based microfluidic platform, named iMµne, was conceived to trap and culture immune cell types, both tissue-resident and circulating, in specific compartments, as well as to assess their cross-talk. The device comprises three PDMS layers (figure 1(a)): (1) a top *Valve layer* hosting actuation mechanisms, (2) a middle *Culture chamber layer*, and (3) a bottom *Unpatterned membrane*. An assembled device is depicted in figure 1(b), together with a picture (figure 1(c)). In detail, the *Culture chamber layer* consists of two separate culture compartments, which are independent at rest, named *3D chamber* and *Sieving valve chamber* (figure 1(d)). The *3D chamber* is designed to host cells (namely resident macrophages) seeded in a 3D matrix and includes a 400 μm-wide central channel suitable for 3D cell-laden fibrin gel injection, flanked by two lateral channels dedicated to culture medium. The central channel is limited by two rows of trapezoidal posts. The *Sieving valve chamber* is a single channel designed to precisely locate, trap and culture immune cells (namely Th1 cells) in suspension. This is achieved by means of the integration of a novel technological solution, named *NC sieving valves,* which builds upon the principles of lifting gate microvalves described from Kim *et al* [31] and curtain valves described from Irimia *et al* [32] In detail, the novelty of the sieving valve technology lies in the integration of an array of underlying microgrooves (height 5 μm) underneath the PDMS wall of a NC curtain valve (figures 1(e) and 2(a–i)). *NC sieving valves* were incorporated at both extremities of the *Sieving valve chamber*. Upon *NC sieving valves* opening through vacuum application (i.e. open position, figure 2(a–ii), PDMS gates located at the extremities of the *Sieving valve chamber* are lifted up, thus allowing both fluid and particles (e.g. cells) to flow into the chamber. Once the valves are closed by removing the negative pressure (i.e. rest position, figure 2(a–iii), PDMS gates are lowered but a smaller passage is still guaranteed owing to underneath microgrooves. As a result, fluidic connection is allowed through the microgrooves, ensuring nutrients exchange through mild perfusion and diffusion, while particles suspended in the fluid remain trapped between the *NC sieving valves*. This mechanism is thus exploited to entrap cells cultured in suspension

within the *Sieving valve chamber*. Initially, both the *NC sieving valves* are opened, and the cell suspension, introduced in one of the two reservoirs, flows inside the *Sieving valve chamber*. Upon closure of both *NC sieving valves*, the fluid velocity suddenly drops, causing the cells to be trapped and avoiding them to be flushed out of the chamber due to residual flow.

Finally, the temporal control of the communication between the two culture compartments is achieved through NC curtain valves [31, 33, 34], named *Communication valves* (figure 2(b)). Unlike *NC sieving valves*, when *Communication valves* are at rest position (figure 2(b–i)), PDMS gates located in- between the two culture compartments completely lay on the underneath PDMS membrane, thus sealing off communication channels and impairing both fluid and cell passage between the compartments. Upon *Communication valves* opening through vacuum application (figure 2(b–ii), video S1), PDMS gates are lifted up and communication between the culture compartments is allowed. The presence of *Communication valves* facilitates an independent stimulation of cells in each compartment using the appropriate culture medium and inflammatory factors, and allowing to selectively initiate their interaction at desired time points.

2.2. Functional validation of *NC Sieving valves*
Sieving valves working mechanism was evaluated by using polystyrene micro-beads (10 μm diameter) to mimic circulating cells behavior in the *Sieving valve chamber* with open *NC sieving valves*, as well as upon valves closure. Briefly, upon *NC sieving valves* opening, beads suspension successfully filled the entire *Sieving valve chamber*. Upon release of the negative pressure, *NC sieving valves* closed properly trapping beads within the *Sieving valve chamber* (video S2). While this result demonstrated the necessity of *NC sieving valves* to properly entrapped cell-like micro-beads inside a chamber, the advantages of *sieving valve* technology (as compared to NC curtain valves) when working with immune cells in suspension was demonstrated in a functional validation test with color dyes. After having seeded beads in the *Sieving valve chamber,* a color dye was used to simulate the addition of culture medium. With open *NC sieving valves*, i.e. simulating a medium change as it is usually performed in standard OoC platforms in absence of such technology, all the beads were immediately flushed away and escaped from the channel (figure 3(a–i), video S3). Contrarily, with closed *NC sieving valves*, beads remained confined in the *Sieving valve chamber*, while a slow but sustained perfusion of dye through the microgrooves was observed over time (figure 3(a–ii), video S4). This demonstrated how with the addition of *NC sieving valves*, immune cells in suspension could not only be trapped, but

Figure 1. Device concept. (a) 3D representation of the different PDMS layers composing the microfluidic platform, i.e. the top *Valve layer* (1), the middle *Culture chamber layer* (2), and the bottom *Unpatterned membrane* (3). (b) 3D representation of the assembled device. (c) Photograph of an assembled device, in which different color dyes have been used to identify the different compartments: yellow for the *3D chamber*, blue for the *Sieving valve chamber* and red for the *Valve layer*. (d) Schematic representation of the device (top view), highlighting *Culture chamber layer* with *3D chamber* (in yellow) and *Sieving valve chamber* (in blue), and *Valve layer* (in red) encompassing *NC sieving* and *communication valves*. A zoom on *NC sieving valve* shows microgrooves (in light blue) at the extremity of the *Sieving valve chamber*, necessary to implement the novel *sieving valve technology*. (e) Schematic representation of the device, showing the novelty of *NC sieving valves,* which lies in the integration of an array of underlying microgrooves (height 5 μm) underneath the PDMS wall of a normally closed curtain valve.
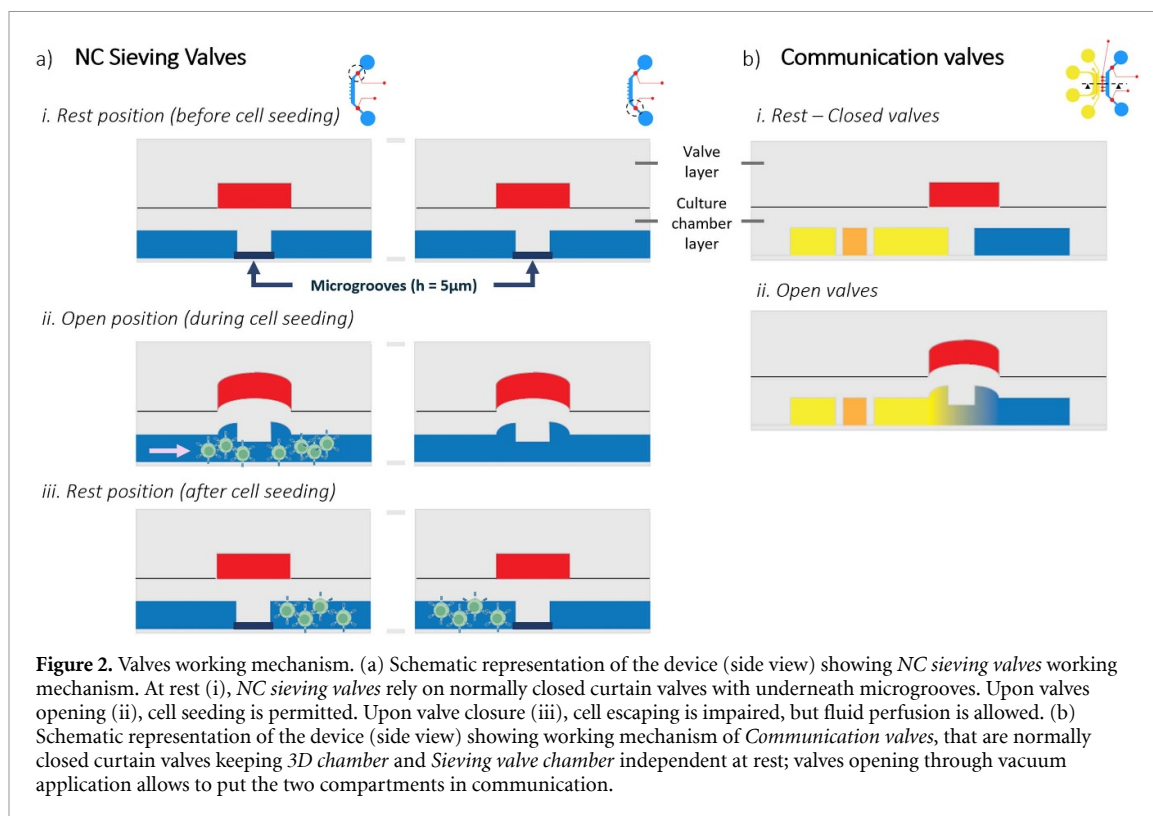
also maintained in culture enabling medium perfusion. Finally, to estimate the time required for the culture medium to reach all the cells in the *Sieving valve chamber*, we utilized a Rhodamine solution. The Rhodamine solution was introduced into the reservoirs while keeping the *NC sieving valves* closed. Fluorescence images taken over time (figure 3(b)) revealed that Rhodamine filled the entire *Sieving valve chamber* within 4 h, indicating that nutrient delivery to all the cells in the chamber is achieved within this time frame.

Moreover, this set-up was used to monitor beads behavior upon communication valves opening, in order to verify that beads were not moving towards the *3D chamber* compartment driven by convection caused by valve opening. Specific tests with color dyes

confirmed that beads migration did not occur when *Communication valves* opened, while slow diffusion of the color dye could be observed proving proper communication between the compartments (figure S1(c)).

2.3. Simulation of a chemoattractant gradient from the *3D chamber* towards the *Sieving valve chamber*

During the onset of RA, release of cytokines and chemokines from synovial cells (i.e. synovial resident macrophages) causes the recruitment and infiltration of circulating cells (e.g. Th1) [13]. Modeling this process *in vitro*, and in general investigating immune cells migration on-chip, crucially requires the establishment of a chemotactic gradient [35].

Figure 2. Valves working mechanism. (a) Schematic representation of the device (side view) showing *NC sieving valves* working mechanism. At rest (i), *NC sieving valves* rely on normally closed curtain valves with underneath microgrooves. Upon valves opening (ii), cell seeding is permitted. Upon valve closure (iii), cell escaping is impaired, but fluid perfusion is allowed. (b) Schematic representation of the device (side view) showing working mechanism of *Communication valves*, that are normally closed curtain valves keeping *3D chamber* and *Sieving valve chamber* independent at rest; valves opening through vacuum application allows to put the two compartments in communication.
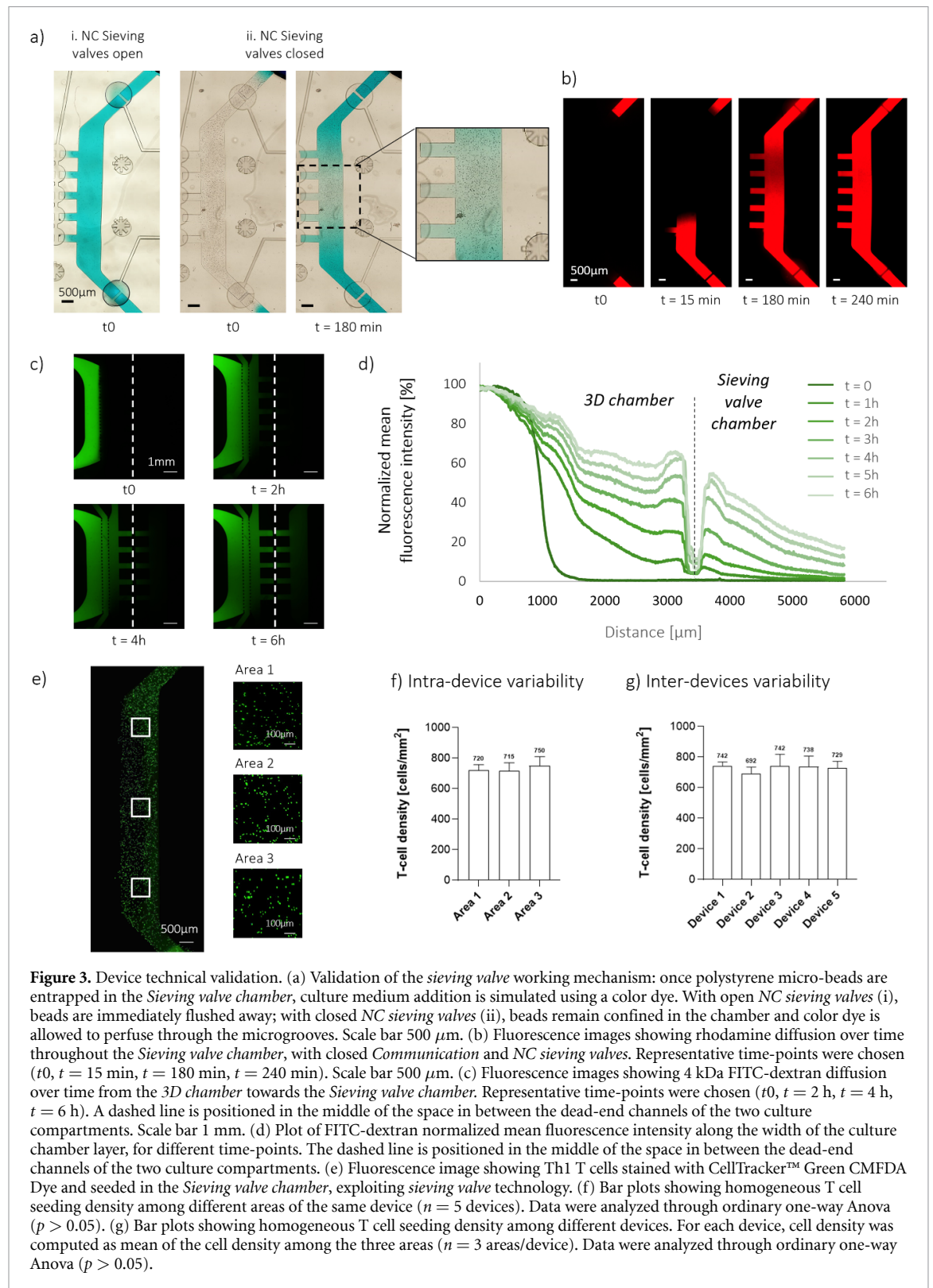
Thus, with the final aim of assessing T cell migration towards pro-inflammatory macrophages, we first evaluated the possibility to generate a chemokine concentration gradient from the *3D chamber* to the *Sieving valve chamber* upon *Communication valves* opening, through the quantification of low molecular weight (4 kDa) FITC-dextran diffusion. Specifically, the central channel of the *3D chamber* was filled with fibrin gel, and 4 kDa FITC-dextran (1.5 mg ml^{-1}) was injected in the outermost medium channel. *Communication valves* were then opened and FITC-dextran diffusion towards the *Sieving valve chamber* was monitored. As shown in figure 3(c), FITC-dextran slowly diffused throughout the entire *3D chamber* in 2 h, while after 4 h its presence could be appreciated also in the *Sieving valve chamber*. Finally, after 6 h, the amount of FITC-dextran in the *Sieving valve chamber* was visibly increased. Plot of normalized mean gray intensity (figure 3(d)) shows a step-like shaped curve at $t = 0$, thus confirming a drop in dextran concentration from the injection channel to the adjacent channel. While the slope of the step-like curve got smoother over-time, the presence of a FITC-dextran gradient was maintained up to 6 h.

2.4. T-cell seeding exploiting *sieving valve* technology

Seeding and culturing of circulating immune cells within microfluidic devices still pose challenges both in terms of reproducible spatial confinement in precise locations and seeding efficiency. Several microfluidic models have been developed over the past years to study the role of the immune system in various physiopathological processes, integrating circulating immune cells [27, 36, 37]. However, most of them rely on perfusion systems, bringing along drawbacks regarding cell loss, applied shear stress that may affect immune cell activation, as well as the need for complex pumping systems. We introduced the *NC sieving valves* technology specifically to address these issues, i.e. enabling precise confinement of a yet limited number of circulating immune cells. *Sieving valves* functionality during seeding and culture of T cell subpopulations was optimized. Briefly, Th1 cells were freshly isolated from human PBMCs derived from healthy donors through magnetic cell separation and fluorescence activated cell sorting (see figure S4 and experimental section for details). Immediately after isolation, Th1 cells were stained with CellTracker™ Green CMFDA Dye for better visualization inside the chip, resuspended in complete RMPI medium (5×10^6 cells ml^{-1}) and injected in the *Sieving valve chamber* with open *NC sieving valves*. Specifically, 4 μl of T cell suspension was injected in each device, corresponding to 20 000 cells, i.e. a number considerably lower than the one needed in previously described devices [25, 26, 29]. Fluorescence images taken in different areas of the same *Sieving valve chamber* showed the achievement of a homogeneous distribution of Th1 cells upon seeding (figure 3(e)), as also confirmed by quantification of cell density (figure 3(f)). Quantification of cell

Figure 3. Device technical validation. (a) Validation of the *sieving valve* working mechanism: once polystyrene micro-beads are entrapped in the *Sieving valve chamber*, culture medium addition is simulated using a color dye. With open *NC sieving valves* (i), beads are immediately flushed away; with closed *NC sieving valves* (ii), beads remain confined in the chamber and color dye is allowed to perfuse through the microgrooves. Scale bar 500 μm. (b) Fluorescence images showing rhodamine diffusion over time throughout the *Sieving valve chamber*, with closed *Communication* and *NC sieving valves*. Representative time-points were chosen ($t0$, $t = 15$ min, $t = 180$ min, $t = 240$ min). Scale bar 500 μm. (c) Fluorescence images showing 4 kDa FITC-dextran diffusion over time from the *3D chamber* towards the *Sieving valve chamber*. Representative time-points were chosen ($t0$, $t = 2$ h, $t = 4$ h, $t = 6$ h). A dashed line is positioned in the middle of the space in between the dead-end channels of the two culture compartments. Scale bar 1 mm. (d) Plot of FITC-dextran normalized mean fluorescence intensity along the width of the culture chamber layer, for different time-points. The dashed line is positioned in the middle of the space in between the dead-end channels of the two culture compartments. (e) Fluorescence image showing Th1 T cells stained with CellTracker™ Green CMFDA Dye and seeded in the *Sieving valve chamber*, exploiting *sieving valve* technology. (f) Bar plots showing homogeneous T cell seeding density among different areas of the same device ($n = 5$ devices). Data were analyzed through ordinary one-way Anova ($p > 0.05$). (g) Bar plots showing homogeneous T cell seeding density among different devices. For each device, cell density was computed as mean of the cell density among the three areas ($n = 3$ areas/device). Data were analyzed through ordinary one-way Anova ($p > 0.05$).

density among areas taken from different devices also showed the absence of statistically significant differences (figure 3(g)), with an average cell density of 728 $\pm$ 19 cells mm^{-2}. These results demonstrate that the proposed *NC sieving valves* allow seeding cells in a controlled way with a high intra- and inter- experiment reproducibility.

2.5. Evaluation of T-cells migration on chip towards a biochemical chemoattractant stimulus

To prove the suitability of the proposed microfluidic platform to study T cell migration from the *Sieving valve chamber* towards the *3D chamber*, a preliminary experiment was performed with a chemoattractant stimulus, with a set-up similar to the one used
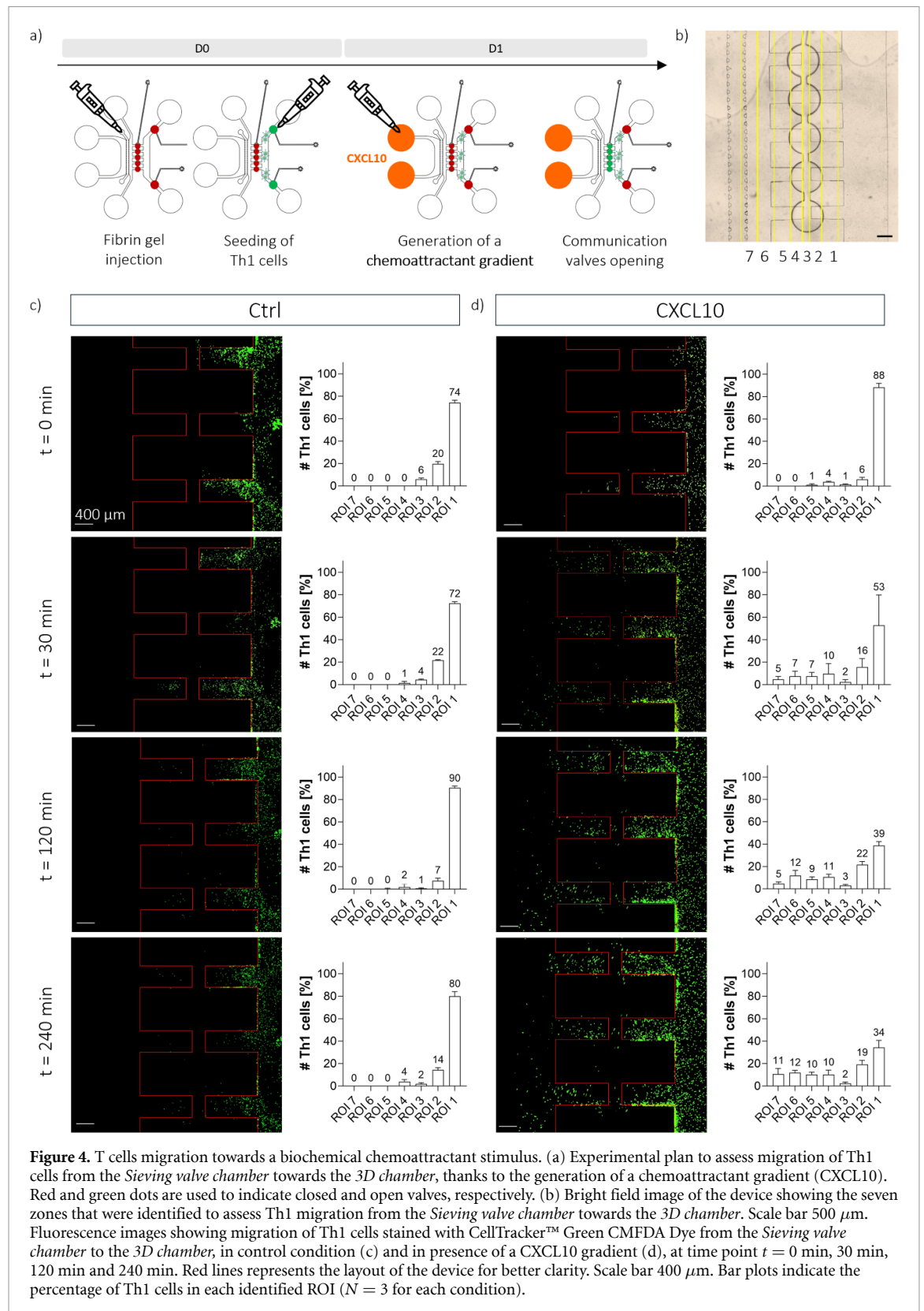
for the FITC-dextran tests. CXCL10 was chosen as chemotactic agent since Th1 cells express CXCR3, the specific receptor for CXCL10 [38]. In details, at day 0, fibrin gel was injected in the central channel of the *3D chamber*; Th1 cells were stained with CellTracker™ Green CMFDA Dye and seeded in the *Sieving valve chamber*. On day 1, CXCL10 (0.5 μg ml^{-1}) was injected in the outermost channel of the *3D chamber* and the migration of Th1 cells was assessed upon *Communication valves* opening (figure 4(a)) through fluorescence microscopy for up to 4 h. Seven regions of interest (ROIs) were identified in the device (figure 4(b)), ranging from the end of the *Sieving valve chamber* (ROI 1) till the center of the *3D chamber* (ROI 7), and cells in each ROI were counted. As shown from fluorescence images (figure 4(c)), no Th1 cells migration was detected right after *Communication valves* opening in the absence of CXCL10 (control condition), thus proving that no cell movement occurs just due to flow convection. Additionally, little Th1 cells migration occurred at later time-points, with few Th1 cells reaching the dead-end channels of the *3D chamber*, and no cells observed in the internal medium channel of the *3D chamber* throughout the entire observation period. These findings are illustrated by bar plots in figure 4(c). At $t = 0$, the percentage of cells in the *3D chamber* (namely ROIs 4, 5, 6, and 7) was zero, with 74% Th1 cells present in ROI 1, and 26% cells distributed among the dead-end channels of the *Sieving valve chamber* and the void space in-between the two culture compartments (namely ROIs 2 and 3). Moreover, at each-time point, the sum of cells in the *Sieving valve chamber* (ROIs 1 and 2) was above 90%, with few cells detected at the entrance of the *3D chamber* (ROI 4: 1%, 2% and 4% for $t = 30$, 120 and 240 min, respectively). The absence of cells in ROIs 5, 6 and 7 at any time point indicated that no cells migrated for a long-distance throughout the *3D chamber*. On the other hand, the addition of CXCL10 induced Th1 cells migration towards the *3D chamber* (figure 4(d)). In details, Th1 cells were observed in the dead-end channels of the *3D chamber* starting from the first time-point, and in the corresponding medium channel after 30 min from the opening of *Communication valves*. In addition, the amount of Th1 cells detectable in the *3D chamber* increased at $t = 120$ and $t = 240$ min. Bar plots support these observations, showing a decreasing percentage of cells over time in the ROI 1, dropping from 88% at $t = 0$, to 53% at $t = 30$ min and 34% at $t = 240$ min. Moreover, the percentage of cells in the dead-end channels of the *3D chamber* (namely ROIs 4 and 5) gradually increased at each time point, with 4% and 1% Th1 cells at $t = 0$ in ROI 4 and 5, respectively, both increasing up to 10% at $t = 240$ min. Finally, no cells were detected in the medium and gel channel of the *3D chamber* (ROIs 6 and 7) at valves opening, while these values increased to 7% and 5%, respectively,

after 30 min, and to 12% and 11%, respectively, at $t = 240$ min. Overall, the continuous decrease of cells in ROI 1 and the continuous increase of cells in ROIs belonging to the *3D chamber* indicated a sustained Th1 migration towards the *Sieving valve chamber*, proving the maintenance of a chemotactic concentration gradient. An estimation of the migration rate is reported in supplementary information (figure S5).

2.6. Macrophage polarization towards pro-inflammatory phenotype M1

Aiming at replicating a known mechanism in RA pathogenesis, characterized by the interaction between CXCL16-expressing resident pro-inflammatory macrophages and CXCR6+ Th1 cells [9], a protocol was established to induce macrophage polarization on-chip towards pro-inflammatory state M1. Briefly, CD14+ monocytes were isolated from human PBMCs derived from a healthy donor, and monocyte-derived macrophages were seeded in the central channel of the *3D chamber*, embedded in a 3D fibrin gel matrix (final cell density 12.5 $\times$ 10^6 cells ml^{-1}). A previously developed protocol [39] was adapted to induce polarization towards pro-inflammatory phenotype M1. In detail, macrophages were stimulated for three days with an inflammatory cocktail composed of 100 ng ml^{-1} TNFα and 100 ng ml^{-1} IFNγ, followed by one day without stimulation. Live/Dead assays were performed at every time point, comparing polarization (M1) and control (M0) conditions, returning a cell viability higher than 76% for every condition (figure S3). The effective polarization of macrophages was investigated by immunofluorescence staining (figure 5(a)) comparing the expression of the pro-inflammatory associated surface markers CD80 and CD86, as well as the synthesis of CXCL16 and MMP1, i.e. proteins relevant in RA mechanisms and synovial inflammation [30, 40], in M1 and M0 conditions, respectively, at day 0, day 3 and day 4. As proven by a statistically significant increase in CD80 and CD86 expression on day 3 in M1 macrophages with respect to M0 controls, macrophages correctly polarized towards pro-inflammatory state after three days of inflammatory stimuli inside the platform (figure 5(b)). Additionally, a statistically significant increase in the secretion of MMP1 and CXCL16 was detected: 18% macrophage synthesized MMP1 at day 0, while 98% were MMP1+ on day 3; CXCL16+ macrophages were 3% and 98% on day 0 and on day 3, respectively. Importantly, these results were also maintained with slight differences one day after removing the inflammatory stimulus, as demonstrated by non-significant differences between M1 samples at day 3 and day 4, indicating that the induced pro-inflammatory phenotype could be maintained stable for at least 24 h.
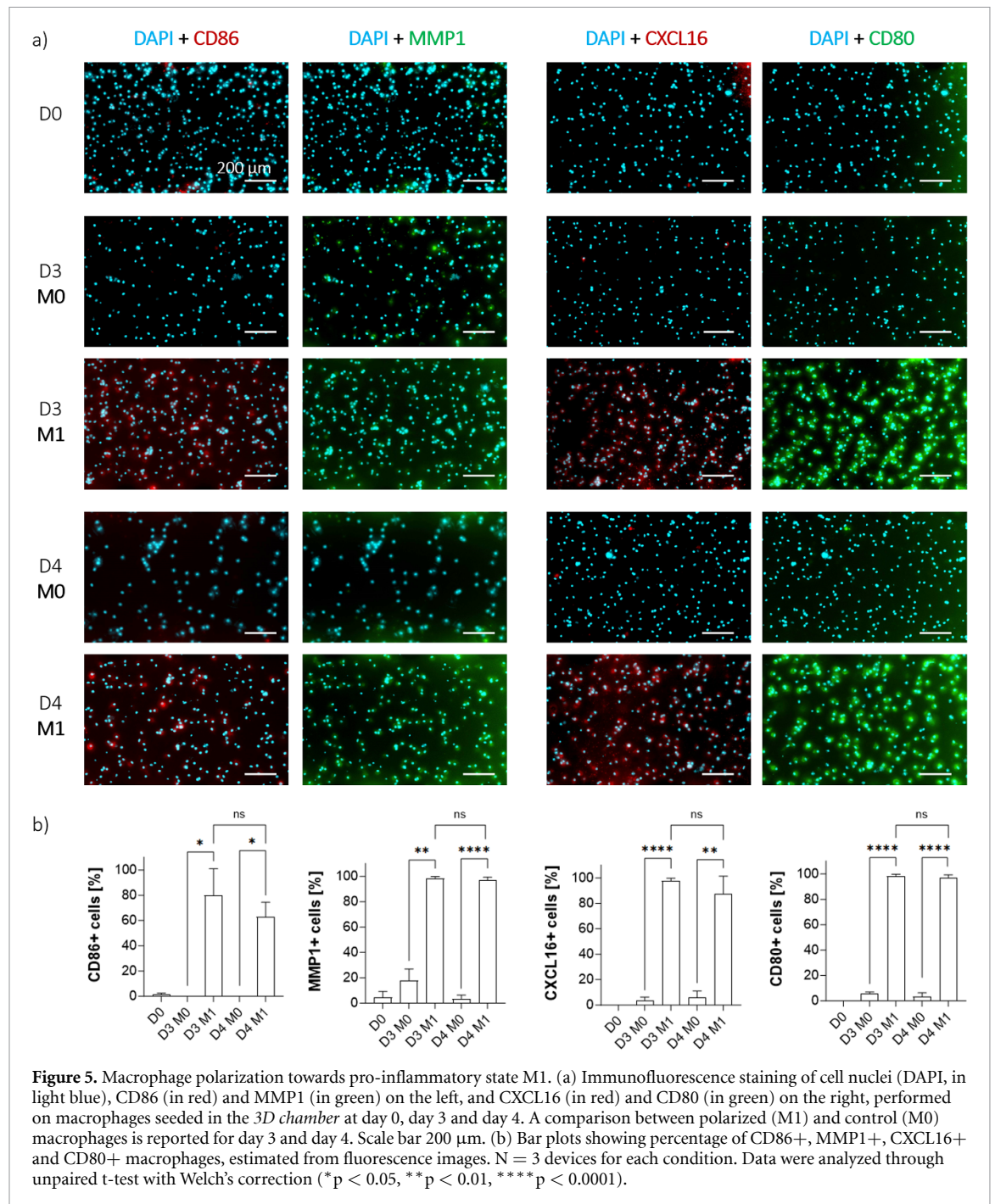
Figure 4. T cells migration towards a biochemical chemoattractant stimulus. (a) Experimental plan to assess migration of Th1 cells from the *Sieving valve chamber* towards the *3D chamber*, thanks to the generation of a chemoattractant gradient (CXCL10). Red and green dots are used to indicate closed and open valves, respectively. (b) Bright field image of the device showing the seven zones that were identified to assess Th1 migration from the *Sieving valve chamber* towards the *3D chamber*. Scale bar 500 μm. Fluorescence images showing migration of Th1 cells stained with CellTracker™ Green CMFDA Dye from the *Sieving valve chamber* to the *3D chamber,* in control condition (c) and in presence of a CXCL10 gradient (d), at time point $t = 0$ min, 30 min, 120 min and 240 min. Red lines represents the layout of the device for better clarity. Scale bar 400 μm. Bar plots indicate the percentage of Th1 cells in each identified ROI ($N = 3$ for each condition).

2.7. Evaluation of T-cell migration on chip towards pro-inflammatory macrophages

Once optimized macrophage culture and polarization in the chip, Th1 migration towards activated macrophages was evaluated [9]. In detail, on day 0, monocyte-derived macrophages were stained with CellTracker™ Orange CMRA Dye and macrophage-laden fibrin gel was injected in the *3D chamber* (figure 6(a)). Two conditions were assessed, whether the pro-inflammatory stimulus previously described was applied (M1) or not (M0). On day 3, Th1 cells stained with CellTracker™ Green CMFDA Dye

Figure 5. Macrophage polarization towards pro-inflammatory state M1. (a) Immunofluorescence staining of cell nuclei (DAPI, in light blue), CD86 (in red) and MMP1 (in green) on the left, and CXCL16 (in red) and CD80 (in green) on the right, performed on macrophages seeded in the *3D chamber* at day 0, day 3 and day 4. A comparison between polarized (M1) and control (M0) macrophages is reported for day 3 and day 4. Scale bar 200 μm. (b) Bar plots showing percentage of CD86+, MMP1+, CXCL16+ and CD80+ macrophages, estimated from fluorescence images. N = 3 devices for each condition. Data were analyzed through unpaired t-test with Welch's correction (*p < 0.05, **p < 0.01, ****p < 0.0001).

were seeded in the *Sieving valve chamber*, following the optimized seeding protocol. On day 4, *Communication valves* were opened to allow cellular cross-talk and Th1 migration was towards M1 or M0 macrophages upon *Communication valves* opening was monitored and quantified as described above. Notably, there was a significant occurrence of Th1 cells migration towards M1 macrophages, denoting the release of chemoattractant stimuli from polarized macrophages. As shown in figure 6(b), at $t = 30$ min Th1 cells started migrating through the communication channels and approaching the medium channel of the *3D chamber* right after valves opening.

Additionally, an increasing number of cells was detected in the *3D chamber,* closer to the macrophage-laden gel channel, in the subsequent time-points. These findings were supported by cell quantification, that displayed a decrease in the cell percentage in the *Sieving valve chamber* (ROIs 1 and 2) during the first 30 min, with values of 48% and 40% at $t = 0$, respectively, and of 30% and 27% at $t = 30$ min, respectively. A corresponding increase of cells that migrated for a long-distance could be observed. In fact, no Th1 cells were detected in the *3D chamber* (ROIs 5, 6 and 7) at $t = 0$, while their presence was 7%, 10% and 3%, respectively, at $t = 30$ min. Moreover,

Figure 6. T cells migration towards pro-inflammatory macrophages. (a) Experimental plan to assess migration of Th1 cells from the *Sieving valve chamber* towards the *3D chamber*, in presence of macrophages polarized to pro-inflammatory state M1. Red and green dots are used to indicate closed and open valves, respectively. Fluorescence images showing migration of Th1 cells stained with CellTracker™ Green CMFDA Dye from the *Sieving valve chamber* to the *3D chamber,* in presence of M1 (b) or M0 (c) macrophages (previously stained with CellTracker™ Orange CMRA Dye), at time point $t = 0$ min, 30 min, 120 min and 240 min. Scale bar 400 μm. Red lines represent the layout of the device for better clarity. Bar plots indicate the percentage of Th1 cells in each identified ROI ($N = 3$ for each condition).

the continuous increase of these values at later time-points confirmed the sustained migration of Th1 towards M1 macrophages due to chemotaxis. In conclusion, M1 macrophage-released chemotactic agents induced a spontaneous and consistent Th1 migration since early time-points, that was sustained during the entire observation period, thus indicating the suitability of the platform to study immune cells crosstalk and migration due to chemoattraction. Remarkably, a migration of Th1 cells occurred also in presence of M0 macrophages (control condition), although only at later time points and in less amount. As noticeable

from fluorescence images in figure 6(c), no cells were present in the *3D chamber* in the first 30 min, while at $t = 120$ min and $t = 240$ min, some Th1 cells were visible in the *3D chamber*. Quantification bar plots corroborated these conclusions, revealing from no to extremely few cells in any ROIs other than ROI 1 and 2 in the first time points (e.g. 54% and 53% Th1 cells in ROI 1, and 0% and 2% in ROI 7 for $t = 0$ and $t = 30$ min, respectively). On the other hand, at later time-points a slow migration of Th1 cells towards M0 macrophages was found (e.g. at $t = 240$ min, 38% Th1 cells were in ROI 1, while 6%, 11% and 4% were in ROI 5, 6 and 7, respectively). Although this is most likely due to the fact that also M0 macrophages secrete an array of cytokines and chemokines that can potentially attract T cells, the number of Th1 cells able to migrate for a long-distance (i.e. within ROIs 4, 5, 6 and 7) in presence of M1 macrophages was always significantly higher than in presence of M0 macrophages (e.g. 4% Th1 cells in ROI 7 at $t = 240$ min in M0 condition, compared to 14% in M1 condition). An estimation of the migration rate is reported in supplementary information (figure S5). Overall, the results of the study indicated that our platform is a promising tool to investigate immune cells interaction and migration in mid-term experiments, working with a limited number of patient-derived cells thanks to the integration of *NC sieving valves*.

To prove the versatility of the platform, a preliminary experiment was also performed by seeding Th17 instead of Th1 cells, demonstrating that also this subpopulation is attracted by pro-inflammatory macrophages (figure S6).

3. Discussion

In a proof-of-concept study aimed at recapitulating the interaction between pro-inflammatory resident macrophages and Th1 cells, we developed a novel microphysiological system, named iMμne, allowing to i) trap and precisely confine T cells with minimal cell loss by means of a sieving valve technology, ii) co-culture them with 3D macrophages and iii) assess macrophages-mediated Th1 cells migration by taking advantages of device compartmentalization.

The immune system assumes a crucial role in preserving tissue homeostasis and coordinating immune responses throughout the evolution of numerous physio-pathological conditions. Within the spectrum of immune-mediated disorders, RA serves a relevant example, with RA synovium containing a diverse array of immune cell types, among which Th1 cells and macrophages are considered key players [41]. Understanding how the cross-talk between these two cell types and their associated cytokines and autoantibodies is involved in RA onset would pave the way to the discovery of efficient reversing treatments for RA [42]. Moreover, RA exhibits significant pathophysiological and clinical heterogeneity,

and individual patient response to drugs can vary significantly [43]. In this scenario, OoC technology offers the opportunity to simulate the tissue-specific microenvironment and investigate disease progression, gaining deeper insights into the complex mechanisms underlying RA pathogenesis. For example, Rothbauer *et al* developed a 3D synovium-on-a-chip system and, using human synovial organoids derived from RA patients' synovial fibroblasts (SFBs), they observed lining hyperplasia and aggregation of SFBs in response to TNFα, indicating a strong inflammatory tissue response [44]. In a subsequent study, Rothbauer *et al* extended their investigation by developing a human joint-on-a-chip model based on co-cultivation of RA patient-derived synovial and chondral organoids, demonstrating significantly elevated cytokine responses, such as IL6 secretion [18]. Ma *et al* developed a microfluidic chip-based platform to co-culture a human SFB cell line (SW982) with osteoclastic RAW264.7 cell line and bone marrow mesenchymal stem cells, replicating SFB migration towards bone cells in RA and modeling SFB-mediated bone erosion [19]. Although these models present the advantage of integrating multiple joint tissues, they lack in modeling the presence of the immune system, necessary for a comprehensive RA investigation.

Envisioning the future goal of recapitulating an immuno-competent joint-on-chip model, in this study we presented the design and fabrication of iMμne, a microfluidic platform aimed at studying the active role of immune system in RA. The platform consists of two distinct and compartmentalized culture areas named *3D chamber* and *Sieving valve chamber*, designated for the culture of macrophages seeded in a 3D matrix and of immune cells in suspension (i.e. Th1 cells), respectively. The culture compartments are independent at rest thanks to normally closed *Communication valves*. The integration of this valve mechanism enables controlled communication between the two compartments, facilitating separate stimulation of cells using the appropriate culture medium and inflammatory factors, and allowing to selectively initiate the interaction between the two cellular populations at desired time points. Moreover, a technological solution was implemented to locate Th1 immune cells in the *Sieving valve chamber*. To enable the possibility to trap and culture few immune cells in suspension with high efficiency and precise control, we introduced a novel valve-based technology, namely *NC sieving valves*, allowing precise confinement of circulating immune cells in the *Sieving valve chamber*, by means of NC curtain valves specifically modified so to integrate underneath microgrooves. In the past years, several microfluidic models have been developed to investigate various immune processes such as neutrophil recruitment [45], immune cell extravasation [46] and monocyte adhesion [47]. However, most of them rely on perfusion systems for introducing

such circulating immune cells inside the microfluidic platforms, resulting in the need of a conspicuous amount of immune cells and missing the capability to precisely control their spatio-temporal location. For example, Huh *et al* exploited a previously developed microfluidic design [48] to recapitulate an immunocompetent alveolus-on-chip. In this study, PBMC were administered to an epithelial channel inlet under flow condition, with need of seeding approximately 1×10^6 cells per chip [29], i.e. 50 times more than in the present study. Moreover, in our model, thanks to the *sieving valve* technology, we could obtain a procedure efficiency of >50% when seeding T cells in the *Sieving valve chamber*, with 10 000 cells remaining confined in the channel of the 20 000 seeded, thus reducing waste of biological material. As a comparison, de Haan *et al* used OrganoPlate, a platform containing 40 microfluidic units underneath a 384-well microtiter plate, to study trans endothelial migration of T cells [28]. A blood vessel structure was recapitulated under perfused conditions, and T cells were added to its lumen to assess adhesion and migration to an adjacent ECM in presence of inflammatory factors. Following this approach, T cell integration exhibited <10% efficiency, with only 200–400 T cells entering the endothelial vessel, over 20 000 cells seeded. Additionally, our seeding protocol allows to collect leftover T cell suspension remaining in the reservoirs of the *Sieving valve chamber* immediately after cell seeding and to seed them in other devices, thus further minimizing cell loss. Moreover, the necessity of integrating the *NC sieving valves* technology when working with immune cells in suspension was further demonstrated in a functional validation test with polystyrene beads and color dyes. After having seeded beads in the *Sieving valve chamber*, a medium change as it is usually performed in standard OoC platforms was simulated with open *NC sieving valves*, causing the immediate escaping of beads from the channel. Contrarily, when *NC sieving valves* were in rest position, the presence of microgrooves allowed perfusing culture medium, while avoiding cell escaping. All these results are particularly relevant when working with patient-derived immune cells obtained from blood samples, as a limited number of cells can be isolated from low volumes of blood, especially when rare cell populations are considered (e.g. rare T cell subsets). The possibility to use the iMµne platform with a low amount of patient-derived immune cells considerably opens up new perspectives towards the concept of patient-specific models to design personalized and targeted therapies, either for RA or many other diseases. Of note, the technology was proven to guarantee homogenous intra- and interdevice seeding density.

Technical validation of the platform demonstrated the proper functioning of the *Sieving* and *Communication valves*, as well as the successful creation of a concentration gradient of FITC-dextran between the *3D chamber* and the *Sieving valve chamber*. In fact, to investigate cellular migration, a chemotactic gradient is necessary. According to literature, currently available microfluidic platforms to create chemotactic gradients are either diffusion-based or perfusion-based systems. On one hand, diffusion-based systems rely on gel barriers or microgrooves to control chemical diffusion of the molecule of interest. However, despite an intrinsic operational simplicity, the lack of control mechanisms causes a fast degradation of the initial chemical gradient, thus limiting their use to short-time experiments [23]. On the other hand, perfusion-based devices rely on continuous perfusion of the chemoattractant, either through pressure-driven or flow-controlled pumping systems. Pressure-driven systems, such as rocking platforms, offer simplicity but have limitations in terms of flow rate control and non-physiological alternating flows. Flow-controlled pumping systems, such as piston-pumps and peristaltic pumps, provide constant and uni-directional flow but may have drawbacks like mechanical stress and bubble formation risk. Moreover, all perfusion-based devices require external equipment, posing challenges related to system complexity and temperature control inside the incubator [20]. By design, the proposed microfluidic platform can be classified as a diffusion-based system, where the insertion of *Sieving valves* increases the hydraulic resistance of the *Sieving valve chamber*, thus limiting convection and slowing down diffusion from one compartment to the other. A gradient of 4 kDa FITC-dextran from the *3D chamber* to the *Sieving valve chamber* could indeed be generated and maintained for up to 6 h, thus making the proposed device suitable for performing medium-term chemotaxis experiments. Since chemokines typically have a molecular weight ranging from 7 to 15 kDa (e.g. CXCL10 has a 8.7 kDa MW) [49], 4 kDa FITC-dextran was selected to simulate a worst-case scenario, as the smaller is the molecule the faster it diffuses from the *3D chamber* to the *Sieving valve chamber*.

To assess the suitability of the platform to study Th1 migration from one compartment to the other, we exploited the possibility to create a stable gradient of a biochemical chemoattractant stimulus. CXCL10 was chosen as chemotactic agent since Th1 cells express CXCR3, the specific receptor for CXCL10 [38]. Notably, a continuous migration of Th1 could be detected from the *3D chamber* towards the *Sieving valve chamber* for the entire observation period, i.e. 4 h, meaning that the chemotactic gradient was maintained. This, together with the absence of migration in control conditions, demonstrated that our platform is adequate to create an environment in which cells can migrate when attracted by a receptor-specific stimulus.

Finally, a comprehensive biological validation was performed, replicating a known mechanism

in RA pathogenesis, characterized by the interaction between CXCL16-expressing resident proinflammatory macrophages and CXCR6+ Th1 cells [9]. Firstly, monocyte-derived macrophages embedded in a fibrin gel matrix were seeded in the *3D chamber* and a previously developed protocol [39] was adapted to induce polarization towards pro-inflammatory phenotype M1. In detail, the experimental plan consisted in three days of pro-inflammatory stimulation (TNFα, IFNγ), followed by one day without stimuli. Proper macrophage activation towards a pro-inflammatory state occurred in the chip as shown by immunofluorescence staining of M1 phenotype clusters of differentiation CD80 and CD86. Moreover, a significant increase was detected in the synthesis of CXCL16 and MMP1, that are relevant proteins in RA synovial inflammation [30, 40]. Interestingly, these results were also maintained one day after stimuli removal. This indicates that the pro-inflammatory phenotype is maintained stable, and in a complete experiment it gives the possibility to open the *Communication valves* to assess macrophage-Th1 interaction on day 4, having removed from the culture medium cytokines that could mask the effect of proteins directly secreted from the macrophages. Once optimized macrophage culture and polarization in the chip, Th1 migration towards activated macrophages was evaluated. In detail, Th1 cells were seeded on day 3 in the *Sieving valve chamber* following the optimized seeding protocol, and *Communication valves* were opened on day 4 to observe their migration in presence of pro-inflammatory (M1) or control (M0) macrophages. As shown from fluorescence images, M1 macrophage-released chemotactic agents induced a spontaneous and consistent Th1 migration since early time-points, that was sustained during the entire observation period, thus indicating the suitability of the platform to study immune cells crosstalk and migration due to chemoattraction. Differently from what expected, Th1 migration occurred also in presence of M0 macrophages, even if in consistently lower number and at later time points. This is most likely due to the fact that also M0 macrophages secrete an array of cytokines and chemokines, that can potentially attract T cells. Further investigations will need to focus on extensively characterizing the different secretome of M0 and M1 macrophages in the chip, e.g. through ELISA, in order to get a deeper insight about the causes of Th1 migration.

While M1 and Th1 interaction is key on RA, pro-inflammatory macrophages have been described to interact also with the rarer Th17 cells, which are attracted to the joint by chemokine ligand CCL20 and its chemokine receptor CCR6 and contribute to sustain the inflammatory positive feedback loop typical of RA [9]. To account for such multi-cellular mechanisms, the platform was also exploited to preliminary investigate Th17 migration towards pro-inflammatory macrophages. Of note, Th17 were

much less abundant than Th1 in the human PBMCs derived from healthy donors, thus resulting in a low cell number available for seeding. In this regard the high seeding efficiency enabled by the *sieving valve* allowed to perform the experiment even in paucity of cells.

Overall, these data indicate that the iMμne platform is a promising tool to investigate immune cells interaction and migration and to work with a limited number of patient-derived cells, thanks to the integration of an innovative valve-based technology. From a technical point of view, the proposed platform presents some limitations, such as low throughput, potentially restricting its application for large-scale studies, and need for experienced operators to fabricate the PDMS-based devices and handle them during biological experiments. Future steps may aim at improving the technology to reduce its complexity and make it more accessible for a broader range of users. From a biological perspective, the current model was realized using healthy PBMCs, which might not fully replicate the pathophysiology of RA. A necessary improvement for the project will involve introducing the comparison with cells derived from RA patients, to enhance the relevance of the model to RA pathophysiology. Moreover, in the view of recapitulating immune cells recruitment operated by RA synovium, SFBs should be integrated in the *3D chamber* as they are considered to play a critical role in perpetuating joint inflammation and damage by producing inflammatory mediators and enzymes [50]. Furthermore, incorporating endothelial cells to the *Sieving valve chamber* could more accurately recreate the physiological microenvironment and study vascular aspects of RA. To conclude, this work presents a promising approach to studying the immune system's role in RA and potentially other diseases. Addressing these limitations and exploring the suggested future steps could significantly enhance its applicability and impact in the field of immunology and personalized medicine.

4. Conclusions

The immune system and its multiple cellular types play a key role in RA, as well as in many other physio-pathological conditions. For this reason, the capability to integrate immune system inside advanced *in vitro* models (e.g. organs-on-chip) is of crucial importance. Here, we developed iMμne, a microfluidic platform that integrates an innovative technological solution, named *NC sieving valve*, to trap a limited number of immune cells inside microfluidic chips and to study their active crosstalk with different cell types, having the possibility to spatio-temporally control their interaction. The platform was here technologically validated and its applicability in studying the cross-talk among different immune cells populations in a pathological scenario like RA was

preliminarily assessed in a proof-of-concept simplified scenario. Specifically, iMµne was exploited to assess short-term Th1 migration in response to a chemotactic agent or in response to the secretome of pro-inflammatory macrophages. Further biological validation will be required to expand the potential of the platform to the recapitulation of the complex multi-cellular inflammatory processes characterizing RA (e.g. integration of different immune cell sub-populations). Next steps will thus involve (i) the extension of the culture over longer time windows of observation to capture chronic events, (ii) the integration of multiple cell types to study key RA mechanisms (e.g. M2-Th2 cross-talk, role of B cells and dendritic cells [7, 12, 51]), and (iii) the combination with more complex micro-scaled joint tissues, e.g. synovium and cartilage [52, 53]. In pursuit of replicating an immune-competent joint-on-chip model, the use of these models will eventually allow elucidating the role of RA patient-derived circulating immune cells on joint tissue degradation, towards the development of patient-specific models to test personalized therapies. Moreover, the *NC sieving valves* technology is highly versatile and can be potentially applied to unravel the interaction between various circulating and tissue-resident immune cells in many diseases also affecting different human districts.

5. Experimental

5.1. Microfluidic device design

The microfluidic platform is composed of three layers of PDMS (Sylgard 184, Dow Corning): a *Valve* layer, a *Culture* chamber layer and an *Unpatterned membrane*. The culture *chamber layer* features two 150 µm-high culture compartments, here named *3D chamber* and *Sieving valve chamber*. The 3D *chamber* is made by a 400 µm-wide central channel for cell-laden hydrogel injection and two lateral medium channels (1100 µm and 700 µm wide, respectively), separated by two rows of pass-through posts with trapezoidal cross-section (main base 160 µm, smaller base 56 µm, height 90 µm), with an inter-post distance of 90 µm within the same row. Central gel channel is provided with two injection ports (1 mm diameter), while each medium channel is provided with medium reservoirs (5 mm diameter) at its ends. On the other side, the *Sieving valve chamber* consists of a single 1330 µm-wide and 150 µm-high channel, having at its extremities two sets of microgrooves (450 µm long, 3 µm wide, 5 µm high), necessary to implement the *sieving valve* technology. The *Sieving valve chamber* is provided with 5 mm-diameter reservoirs. The two chambers are separated by five 1000×400 µm dead-end channels where PDMS walls (250×400 µm wide) are generated to isolate the two compartments. The valve layer features two sets of valves (150 µm high). *Communication valves* consist of a line of five interconnected rounded cavities (1 mm diameter)

aligned on top of the PDMS walls separating the culture compartment. *NC sieving valves* consist of two rounded cavities (1.5 mm diameter) aligned on top of the two sets of microgrooves in the *Sieving valve chamber*. Access to valves is guaranteed through 1.5 mm holes.

5.2. Microfluidic device fabrication

The devices were realized through soft-lithography of PDMS on SU-8 master moulds (Microchem). In detail, layouts containing the desired geometric features for the *Valve* and *Culture chamber layers* were realized using computer-assisted design (CAD) software (AutoCAD, Autodesk Inc.). CAD drawings were then used to fabricate master molds through photolithography in a cleanroom environment (Polifab, Politecnico di Milano). Briefly, SU-8 photoresist was spin-coated onto 4-inch silicon wafers, in order to obtain the desired height, and features pattern was transferred on the wafer through laser light exposure (Maskless Aligner MLA100, Heidelberg Instruments). Multi-layer photolithography was used for the fabrication of the chamber layer mould, first realizing microgrooves (5 µm high), and subsequently exposing a 150 µm SU-8 layer to obtain the remaining features. Single-layer photolithography was used for the generation of valve layer (150 µm high). Following exposure, silicon wafers were cured and developed according to the manufacturer's specification, thus obtaining master molds with features in relief. The microstructure master molds were then employed for the soft-lithographic process. Initially, master mold surfaces were exposed to tri-methyl-chloro-silane (Sigma-Aldrich) for 30 min at room temperature (RT), in order to prevent PDMS from adhering to the wafer and facilitate its removal. PDMS layers were then casted through replica molding of the master molds. In detail, a mixture of PDMS and curing agent at a 10:1 ratio (Sylgard 184, Dow Corning) was poured on the molds and polymerized at 65 °C for at least 3 h. In particular, a defined amount of PDMS was poured on the chamber layer master mold, in order to obtain a controlled thickness (300 µm) to guarantee valves functioning. After cross-linking, PDMS stamps were peeled off from the silicon wafers, and access ports on the *Valve layer* were obtained using a 1.5 mm biopsy puncher. Thus, *Valve layer* and *Culture chamber layer* underwent a plasma treatment (Harrick Plasma Inc.) and were brought into conformal contact (figures S1(a) and (b)) to achieve irreversible bonding after 15 min at 65 °C. After bonding, the assembly was finalized by punching circular access ports with biopsy punchers (5 mm for *3D chamber* and *Sieving valve chamber* reservoirs, 1 mm for *3D chamber* gel injection ports). Finally, a PDMS membrane was fabricated with a thickness of 500 µm by accurately dousing the PDMS poured on a flat substrate, and the microfluidic platform was completed by plasma bonding

the chamber-valve assembly onto the PDMS membrane. To produce microfluidic devices with functioning *Sieving* and *Communication valves*, this last step was performed under vacuum condition. In details, three Tygon tubes (Qosina) were inserted in the valves access ports and connected to a vacuum chamber at -0.8 bar prior to bonding, thus guaranteeing valve opening during bonding procedure and avoiding permanent bonding of the separating walls on the membrane.

5.3. *NC sieving valves* technical validation

After design and fabrication, the novel *sieving valve* technology was functionally validated. A suspension of spherical polystyrene beads (diameter = 10 μm, Merck) in PBS was used to simulate cell behaviour. The mechanism was questioned in two configurations, i.e. with open *NC sieving valves*, when cell passage is expected, and with closed *NC sieving valves*, i.e. when no cell passage, but fluid perfusion is expected. In details, *NC sieving* and *Communication valves* were open, and the entire device was filled with PBS, to avoid air bubbles formation in the communication channels. Subsequently, *Communication valves* were closed and every reservoir was emptied from PBS. A 50 μl solution composed of PBS, 10% microbeads and 10% Tween® 20 (Sigma Aldrich) was then added in the inlet reservoir of the *Sieving valve chamber* (video S2). Once the beads had filled all the channel, *NC sieving valves* were closed by applying a positive pressure of 0.6 bar, and the inlet and outlet reservoirs were emptied from the remaining beads solution. Hence, a solution of 20% color dye and 10% Tween® 20 in PBS was used to simulate the addition of culture medium in the *Sieving valve chamber*, comparing open and rest valve position (video S3, video S4). The colored solution was injected in the reservoirs of the *Sieving valve chamber*, either maintaining *NC sieving valves* closed or opening them through vacuum application. Sieving valve mechanism was evaluated in terms of dye diffusion over time and beads escaping throughout the channel, observing the device through an inverted microscope (Olympus IX83). To estimate the time required for nutrients to reach the entire *Sieving valve chamber*, the same experiment was performed with a Rhodamine solution. Specifically, a solution of 1.5 mg ml^{-1} RFP-Rhodamine (Alquera) in PBS was injected in the reservoirs of the *Sieving valve chamber*, while keeping *NC sieving valves* closed. Rhodamine diffusion throughout the channel was monitored using a fluorescence microscope during a 240 min timeframe.

5.4. *Communication valves* technical validation

The entire device was primed with PBS, keeping both *Communication* and *NC sieving valves* open. After closing the *Communication valves*, inlet and outlet reservoirs of the medium channels of the *3D chamber* were first emptied from PBS and then filled with a yellow color dye. PBS was then removed from the inlet and outlet reservoirs of the *Sieving valve chamber*, that were subsequently filled with a solution of beads and blue color dye (PBS, 20% color dye, 10% microbeads, 1% Tween® 20). Finally, *NC sieving valves* were closed and *Communication valves* were opened, and beads movement was observed through an inverted microscope.

5.5. Evaluation of FITC-dextran diffusion

The following experimental set-up was used to quantify the diffusion of low molecular weight (4 kDa) FITC-dextran (Sigma Aldrich). The central channel of the *3D chamber* was injected with fibrin gel (fibrinogen 10 mg ml^{-1}, thrombin 2.5 U ml^{-1}) and, after cross-linking (10 min at 37 °C), all the channels were primed with PBS, maintaining all valves open. *NC sieving valves* were then closed and all the reservoirs filled with 70 μl PBS, with the exception of the reservoirs of the outermost medium channel of the *3D chamber*. At $t = 0$, inlet and outlet reservoirs of the outermost medium channel of the *3D chamber* were filled with 70 μl 4 kDa FITC-dextran (1.5 mg ml^{-1} in PBS), and *Communication valves* were opened. FITC-dextran diffusion was observed through an inverted microscope: representative images were taken every 5 min for the first 40 min, and every 10 min up to 6 h. Additionally, images were analyzed through ImageJ software, to quantify FITC-dextran fluorescence intensity in the device over time. Specifically, each image was converted into a 8-bit image and gray intensity values were computed on 5 linear ROIs, identified along the axes of the five communication valves (figure S2): for each of the five channels, the intensity of the gray value was computed from the outermost limit of the *3D chamber* to the outermost limit wall of the *Sieving valve chamber*. Gray values for each ROI were then normalized against the maximum gray value of the axis. Mean gray intensity was thus obtained averaging the values computed in the 5 ROIs, and reported in a graph for representative timepoints to visualize the trend of FITC-dextran concentration gradient over time.

5.6. Cell harvesting and isolation

Untouched CD4+ memory T helper cells were negatively isolated from human PBMCs with Memory CD4+ T Cell Isolation Kit (Miltenyi Biotech), according to manufacturer's instructions. CD4+ memory T cells were further FACS-sorted using live (BV510), CD4 (PE), CCR6 (BV786), CD45RO (PE Cy7), CCR4 (BV421), CXCR3 (PerCP5.5), CD161 (BV605).

Th1 and control T cells were defined according to the following gating strategy: T helper 1 (CD4 + CD45RO + CCR6-CCR4-CXCR3highCD161-) and CTRL (CD4 + CD45RO + CCR6 + CCR4-CXCR3lowCD161-) cells. Purity of isolated human T cell populations were checked by

FACS (>95%). Th1 and control T cells were further characterized by FACS for cytokines production. Both T cell subsets (Th1 and CTRL T cells) were stimulated post sorting with PMA and ionomycin in the presence of Golgi Plug. Cells were further stained with fluorochrome conjugated antibodies specific for IFNγ (APC Cy7), TNFα (BV786) and IL17A (FITC) and analyzed by flow cytometry. Human CD14+ monocytes were purified according to manufacturer's instructions using CD14+ Isolation Kit Mouse (Miltenyi Biotech) and purity was checked by FACS (>95%).

5.7. T-cell seeding in the iMµne platform

After isolation, T cells were stained with Celltracker^{TM} Green (ThermoFisher) according to manufacturer's protocol and resuspended in RPMI complete medium, i.e. RPMI-1640, 10% v/v fetal bovine serum (FBS, Hyclone), 1% GlutaMAX^{TM} supplement, 1% MEM Non-Essential Amino Acids Solution, 1% Sodium Pyruvate, 1% HEPES Buffer, 1% Penicillin- Streptomycin (ThermoFisher), to reach a final concentration of 5×10^6 cells ml^{-1}. After having primed the devices with RPMI only, *Communication valves* were closed and 4 μl of T cell suspension, corresponding to 20 000 cells, were seeded as it follows. *NC sieving valves* were opened through vacuum application and inlet and outlet reservoirs of the *Sieving valve chamber* were emptied. A 2 μl droplet of cell suspension was put in the inlet of the *Sieving valve chamber*. After 10 s, an additional 2 μl cell suspension droplet was put in the outlet, and other 10 s were waited. Afterwards, a volume of 2 μL was taken from the inlet and injected in the outlet. After 10 s, the same procedure was done from the outlet to the inlet. The same procedure was performed one other time. *NC sieving valves* were then closed by applying 0.6 bar. Remaining cells in the inlet and outlet reservoirs were collected and complete RPMI complete medium was added to each reservoir (50 μl/reservoir). After seeding, fluorescence images of the *Sieving valve chamber* were taken for five devices through an inverted microscope, and mean cell density was computed through ImageJ software considering three square ROIs along the chamber (figure 3(e)).

5.8. T cell migration on chip towards a biochemical chemoattractant stimulus

At day 0, fibrin gel (fibrinogen 10 mg ml^{-1}, thrombin 2.5 U ml^{-1}) was injected in the central channel of the *3D chamber*. After gel polymerization, all the channels were filled with RPMI-1640, and freshly isolated Th1 cells pre-stained with Celltracker^{TM} Green were seeded in the *Sieving valve chamber*, following the above-described protocol. Thus, to generate a gradient of the supplied stimulus from the *3D chamber* towards the *Sieving valve chamber*, all the reservoirs were filled with 70 μl of complete RPMI

medium, with the exception of the reservoirs of the outermost channel of the *3D chamber*, keeping all the valves closed. The inlet and outlet reservoirs of the outermost medium channel were then filled with 70 μl CXCL10 solution (0.5 μg ml^{-1} in complete RPMI medium) or complete RPMI medium (control condition). *Communication valves* were then opened and T cell migration evaluated through an inverted microscope. Fluorescence images were taken for each device every 5 min for the first half hour, and every 30 min for the subsequent 210 min. To quantify cell migration, the device was divided into seven ROIs (figure 4(b)). Specifically, ROIs 1 and 2 correspond to the dead-end channels of the *Sieving valve chamber*, ROI 3 corresponds to the void space between the *Sieving valve chamber* and the *3D chamber*, and ROIs 4, 5, 6 and 7 belong to the *3D chamber*. For each ROI cells were counted automatically through ImageJ software. Values were then normalized by the total number of cells in all the ROIs and results were averaged among $n = 3$ devices per condition, for each timepoint.

5.9. 3D macrophage culture and polarization in the device

Human CD14+ monocytes were purified from PBMCs derived from a healthy donor using CD14+ Isolation Kit Mouse (Miltenyi Biotech) according to manufacturer's instructions. Purity was checked by FACS (>95%). Freshly isolated CD14+ monocytes (i.e. at passage 0) were then pre-differentiated towards macrophages in flask for five days in complete RPMI medium, supplemented with 20 ng ml^{-1} macrophage colony-stimulating factor (MCSF, R&D Systems), in a humified incubator. Afterwards, suspended macrophages were collected and adhered macrophages were detached by incubating them at 37 °C for 5 min in Cell Dissociation Buffer (ThermoFisher). After cell count and centrifuging, macrophages were suspended in a 10 mg ml^{-1} fibrin gel (fibrinogen 10 mg ml^{-1}, thrombin 2.5 U ml^{-1}) at a cell density of 12.5×10^6 cells ml^{-1}, and seeded in the gel channel of the *3D chamber*. After cell-laden gel cross-linking, that occurred in a humified incubator (5% CO$_2$, 37 °C) for 8 min, adjacent medium channels were filled with RPMI complete medium, supplemented with factors as follows. In details, macrophages in control condition (M0) were supplemented with 20 ng ml^{-1} MCSF, while macrophages to be polarized towards pro-inflammatory state (M1) were supplemented with 20 ng ml^{-1} MCSF, 100 ng ml^{-1} IFNγ (R&D Systems) and 100 ng ml^{-1} TNFα (R&D Systems) [39]. In both conditions, culture medium was supplemented with 2 mg ml^{-1} aminocaproic acid (ACA, Sigma-Aldrich), that was gradually decreased during the culture period (day 2 1.6 mg ml^{-1}, day 3 1.4 mg ml^{-1}). On day 3, pro-inflammatory stimuli were removed from M1 macrophages, to assess whether the pro-inflammatory phenotype can be

maintained stable. Macrophage culture in the chip was carried out up to day 4. On day 0, 3 and 4, samples were collected for viability assays and immunofluorescence, as described below.

5.10. Viability assay

On day 0, 3 and 4, a viability assessment was performed on macrophages seeded in the chip using a Live/Dead assay (Sigma-Aldrich). The devices were washed three times with PBS and subsequently incubated in the dark at 37 °C for 15 min with a solution containing calcein (2 μm) and ethidium homodimer-1 (4 μm). After rinsing with PBS, fluorescent images of 3 devices per condition were captured using an inverted microscope. To quantify cell viability, ImageJ software was employed. Three ROIs were selected for each device, and within each ROI the green labelled cells (indicating live cells) and the red cell nuclei (indicating dead cells) were counted. Cell viability values were thus obtained by normalizing the number of alive cells against the total number of cells. Mean and standard deviation values were finally calculated for cell viabilities and plotted for each experimental condition.

5.11. Immunofluorescence staining

Before fixation, chambers were incubated for 4 h at 37 °C with appropriate culture medium supplemented with Brefeldin A (Abcam), to inhibit protein transport processes and increase intracellular protein staining signals. Afterward, chambers were washed twice with PBS and incubated for 30 min at RT with paraformaldehyde 4%. Following fixation procedure, cells were rinsed with PBS and permeabilized with 0.5% Triton-X (Sigma-Aldrich) for 10 min at RT. A blocking solution, containing 3% goat serum and 0.3% Tween® 20 in PBS, was then applied for 1 h at RT to block non-specific bindings. Samples were then incubated overnight at 4 °C with primary antibody solution, containing primary antibodies at the desired dilution in blocking solution. In detail, a first staining was performed using rabbit anti-human CD80 (dilution 1:1000, Abcam) and mouse anti-human CXCL16 (dilution 1:1000, GeneTex), while a second staining was performed with mouse anti-human CD86 (dilution 1:200, SantaCruz) and rabbit anti-human MMP1 (dilution 1:1000, Abcam). The following day, samples were rinsed with blocking solution and incubated for 2 h at RT in the dark with appropriate secondary antibody solution, containing 488 Goat Anti-Rabbit IgG (dilution 1:200, ThermoFisher) and 546 Goat Anti-Mouse IgG1 (dilution 1:200, ThermoFisher). Following rinse with PBS, samples were finally incubated for 30 min at RT with nuclear staining solution (DAPI, 300 nM). Fluorescence images were taken with inverted microscope and analyzed through ImageJ software. CD80,

CXCL16, CD86 and MMP1-expressing cells were identified by co-localizing staining signals with cell nuclei, and normalized over the number of total cells. The percentage of expressing cells were compared using GraphPad Prism. Additionally, an unstained control group was prepared as follows: after permeabilization and blocking of non-specific binding sites, the samples were incubated with either a solution of 488 Goat Anti-Rabbit IgG (1:200) or 546 Goat Anti-Mouse IgG1 (1:200). After rinsing with PBS, the samples were incubated with DAPI (300 nM). Corresponding fluorescence images are reported in supplementary information (figure S3(c)).

5.12. Evaluation of T-cells migration on chip towards polarized macrophages

After five days of pre-differentiation, macrophages were stained with CellTracker™ Orange (ThermoFisher) according to manufacturer's specifications and cell-laden fibrin gel was injected in the *3D chamber* as described in the previous sections (day 0). After gel cross-linking, medium channels of the *3D chamber* were filled with appropriate culture medium, i.e. either complete RPMI supplemented with 20 ng ml^{-1} MCSF and 2 mg ml^{-1} ACA (M0, $n = 3$), or complete RPMI medium supplemented with 2 mg ml^{-1} ACA, 20 ng ml^{-1} MCSF, 100 ng ml^{-1} IFNγ and 100 ng ml^{-1} TNFα (M1, $n = 3$). On day 3, Th1 cells stained with CellTracker™ Green were seeded in the *Sieving valve chamber*, following the previously validated protocol, and a medium change was performed in the *3D chamber* to remove pro-inflammatory stimuli (complete RPMI supplemented with 20 ng ml^{-1} MCSF and 1.4 mg ml^{-1} ACA). On day 4, *Communication valves* were opened to allow cellular cross-talk and Th1 migration was observed through inverted microscope. Fluorescence images were taken and analyzed as described above, to quantify Th1 migration over time.

5.13. Statistical analysis

Statistical analyses were performed using GraphPad Prism software. Once verified that data distribution were normally distributed using Kolmogorov–Smirnov test, multiple comparisons were realized using ordinary one-way analysis of variance (ANOVA), while unpaired t-test with Welch's correction was used when comparing two normally-distributed populations.

Data availability statement

All data that support the findings of this study are included within the article (and any supplementary files).

Acknowledgment

Conflict of interest

The authors declare no conflict of interest.

Ethical statement

The collection of samples from healthy donors has been approved by the IEO's Ethical Committee (registered as IEO 1781). All donors provided written informed consent in accordance with the Declaration of Helsinki.

ORCID iDs

Cecilia Palma ⦿ https://orcid.org/0000-0001-9517-1803
Bianca Aterini ⦿ https://orcid.org/0009-0008-0963-8365
Erika Ferrari ⦿ https://orcid.org/0000-0003-3863-0596
Marta Mangione ⦿ https://orcid.org/0009-0001-0227-9637
Martina Romeo ⦿ https://orcid.org/0009-0000-5897-8165
Luigi Nezi ⦿ https://orcid.org/0000-0002-4670-7656
Silvia Lopa ⦿ https://orcid.org/0000-0003-0410-5814
Teresa Manzo ⦿ https://orcid.org/0000-0001-8552-3625
Paola Occhetta ⦿ https://orcid.org/0000-0002-5758-2019
Marco Rasponi ⦿ https://orcid.org/0000-0002-2904-8652

References

[1] Weisberg S P, Ural B B and Farber D L 2021 Tissue-specific immunity for a changing world *Cell* **184** 1517–29
[2] Smolen J S *et al* 2018 Rheumatoid arthritis *Nat. Rev. Dis. Primers* **4** 18001
[3] Wu C-Y, Yang H-Y and Lai J-H 2020 Anti-citrullinated protein antibodies in patients with rheumatoid arthritis: biological effects and mechanisms of immunopathogenesis *Int. J. Mol. Sci.* **21** 4015
[4] Lee D M and Weinblatt M E 2001 Rheumatoid arthritis *Lancet* **358** 903–11
[5] Firestein G S 2003 Evolving concepts of rheumatoid arthritis *Nature* **423** 356–61
[6] Yap H-Y, Tee S, Wong M, Chow S-K, Peh S-C and Teow S-Y 2018 Pathogenic role of immune cells in rheumatoid arthritis: implications in clinical treatment and biomarker development *Cells* **7** 161
[7] Cutolo M, Campitiello R, Gotelli E and Soldano S 2022 The role of M1/M2 macrophage polarization in rheumatoid arthritis synovitis *Front. Immunol.* **13** 867260
[8] Zheng Y *et al* 2024 Macrophage polarization in rheumatoid arthritis: signaling pathways, metabolic reprogramming, and crosstalk with synovial fibroblasts *Front. Immunol.* **15** 1394108
[9] Roberts C A, Dickinson A K and Taams L S 2015 The interplay between monocytes/macrophages and CD4+ T cell subsets in rheumatoid arthritis *Front. Immunol.* **6** 571
[10] Kinne R W, Bräuer R, Stuhlmüller B, Palombo-Kinne E and Burmester G-R 2000 Macrophages in rheumatoid arthritis *Arthritis Res. Ther.* **2** 189
[11] Yang X, Chang Y and Wei W 2020 Emerging role of targeting macrophages in rheumatoid arthritis: focus on polarization, metabolism and apoptosis *Cell Proliferation in basic and clinical sciences* **53** e12854
[12] Luo P, Wang P, Xu J, Hou W, Xu P, Xu K, Liu L and Xu P 2022 Immunomodulatory role of T helper cells in rheumatoid arthritis *Bone Joint Res.* **11** 426–38
[13] Tu J, Huang W, Zhang W, Mei J and Zhu C 2021 A tale of two immune cells in rheumatoid arthritis: the crosstalk between macrophages and T cells in the synovium *Front. Immunol.* **12** 655477
[14] Damerau A and Gaber T 2020 Modeling rheumatoid arthritis in vitro: from experimental feasibility to physiological proximity *Int. J. Mol. Sci.* **21** 7916
[15] Paggi C A, Teixeira L M, Le Gac S and Karperien M 2022 Joint-on-chip platforms: entering a new era of in vitro models for arthritis *Nat. Rev. Rheumatol.* **18** 217–31
[16] Morsink M, Willemen N, Leijten J, Bansal R and Shin S 2020 Immune organs and immune cells on a chip: an overview of biomedical applications *Micromachines* **11** 849
[17] Ferrari E, Palma C, Vesentini S, Occhetta P and Rasponi M 2020 Integrating biosensors in organs-on-chip devices: a perspective on current strategies to monitor microphysiological systems *Biosensors* **10** 110
[18] Rothbauer M *et al* 2021 Establishment of a human three-dimensional chip-based chondro-synovial coculture joint model for reciprocal cross talk studies in arthritis research *Lab Chip* **21** 4128–43
[19] Ma H-P, Deng X, Chen D-Y, Zhu D, Tong J-L, Zhao T, Ma J-H and Liu Y-Q 2018 A microfluidic chip-based co-culture of fibroblast-like synoviocytes with osteoblasts and osteoclasts to test bone erosion and drug evaluation *R Soc. Open Sci.* **5** 180528
[20] Van Os L, Engelhardt B and Guenat O T 2023 Integration of immune cells in organs-on-chips: a tutorial *Front. Bioeng. Biotechnol.* **11** 1191104
[21] Miller C P, Shin W, Ahn E H, Kim H J and Kim D-H 2020 Engineering microphysiological immune system responses on chips *Trends Biotechnol* **38** 857–72
[22] Irimia D and Wang X 2018 Inflammation-on-a-chip: probing the immune system *ex vivo Trends Biotechnol.* **36** 923–37
[23] Zhao W, Zhao H, Li M and Huang C 2020 Microfluidic devices for neutrophil chemotaxis studies *J. Transl. Med.* **18** 168
[24] Tiberti S *et al* 2022 GZMKhigh CD8+ T effector memory cells are associated with CD15high neutrophil abundance in non-metastatic colorectal tumors and predict poor clinical outcome *Nat. Commun.* **13** 6752
[25] Pavesi A *et al* 2017 A 3D microfluidic model for preclinical evaluation of TCR-engineered T cells against solid tumors *JCI Insight* **2** 89762
[26] van Os L, Yeoh J, Witz G, Ferrari D, Krebs P, Chandorkar Y, Zeinali S, Sengupta A and Guenat O T 2023 Immune cell

extravasation in an organ-on-chip to model lung inflammation *Eur. J. Pharm. Sci.* **187** 106485

[27] Leung C M *et al* 2022 A guide to the organ-on-a-chip *Nat. Rev. Method Primers* **2** 33

[28] de Haan L *et al* 2021 A microfluidic 3D endothelium-on-a-chip model to study transendothelial migration of T cells in health and disease *Int. J. Mol. Sci.* **22** 8234

[29] Kerns S J *et al* 2021 Human immunocompetent organ-on-chip platforms allow safety profiling of tumor-targeted T-cell bispecific antibodies *Elife* **10** e67106

[30] Nanki T, Shimaoka T, Hayashida K, Taniguchi K, Yonehara S and Miyasaka N 2005 Pathogenic role of the CXCL16–CXCR6 pathway in rheumatoid arthritis *Arthritis Rheumatol.* **52** 3004–14

[31] Kim J, Kang M, Jensen E C and Mathies R A 2012 Lifting gate polydimethylsiloxane microvalves and pumps for microfluidic control *Anal. Chem.* **84** 2067–71

[32] Irimia D, Liu S-Y, Tharp W G, Samadani A, Toner M and Poznansky M C 2006 Microfluidic system for measuring neutrophil migratory responses to fast switches of chemical gradients *Lab Chip* **6** 191–8

[33] Visone R, Ugolini G S, Vinarsky V, Penati M, Redaelli A, Forte G and Rasponi M 2019 A simple vacuum-based microfluidic technique to establish high-throughput organs-on-chip and 3D cell cultures at the microscale *Adv. Mater. Technol.* **4** 1800319

[34] Ferrari E, Visone R, Monti E, Torretta E, Moretti M, Occhetta P and Rasponi M 2023 LivHeart: a multi organ-on-chip platform to study off-target cardiotoxicity of drugs upon liver metabolism *Adv. Mater. Technol.* **8** 2201435

[35] Vesperini D, Montalvo G, Qu B and Lautenschläger F 2021 Characterization of immune cell migration using microfabrication *Biophys. Rev.* **13** 185–202

[36] Ramadan Q, Hazaymeh R and Zourob M 2023 Immunity-on-a-chip: integration of immune components into the scheme of organ-on-a-chip systems *Adv. Biol.* **7** 2200312

[37] Polini A, Del Mercato L L, Barra A, Zhang Y S, Calabi F and Gigli G 2019 Towards the development of human immune-system-on-a-chip platforms *Drug Discovery Today* **24** 517–25

[38] Elemam N M, Hannawi S and Maghazachi A A 2020 Role of chemokines and chemokine receptors in rheumatoid arthritis *Immunotargets Ther.* **9** 43–56

[39] Mondadori C, Chandrakar A, Lopa S, Wieringa P, Talò G, Perego S, Lombardi G, Colombini A, Moretti M and Moroni L 2023 Assessing the response of human primary macrophages to defined fibrous architectures fabricated by melt electrowriting. *Bioact. Mater.* **21** 209–22

[40] Peck Y, Leom L T, Low P F P and Wang D-A 2018 Establishment of an in vitro three-dimensional model for cartilage damage in rheumatoid arthritis *J. Tissue Eng. Regen. Med.* **12** e237–49

[41] McInnes I B and Schett G 2011 The pathogenesis of rheumatoid arthritis *New Engl. J. Med.* **365** 2205–19

[42] Wajid Ali Khan M and Ali Khan W 2019 Autoantibodies and Cytokines in Pathogenesis of Rheumatoid Arthritis *Autoantibodies and Cytokines* (IntechOpen) (https://doi.org/10.5772/intechopen.82265)

[43] Zhao J, Guo S, Schrodi S J and He D 2021 Molecular and Cellular Heterogeneity in Rheumatoid Arthritis: Mechanisms and Clinical Implications *Front. Immunol.* **12** 790122

[44] Rothbauer M *et al* 2020 Monitoring tissue-level remodelling during inflammatory arthritis using a three-dimensional synovium-on-a-chip with non-invasive light scattering biosensing *Lab Chip* **20** 1461–71

[45] Benam K H *et al* 2016 Small airway-on-a-chip enables analysis of human lung inflammation and drug responses in vitro *Nat. Methods* **13** 151–7

[46] Mondadori C, Crippa M, Moretti M, Candrian C, Lopa S and Arrigoni C 2020 Advanced microfluidic models of cancer and immune cell extravasation: a systematic review of the literature *Front. Bioeng. Biotechnol.* **8** 907

[47] Poussin C *et al* 2019 3D human microvessel-on-a-chip model for studying monocyte-to-endothelium adhesion under flow—application in systems toxicology *Altern. Animal Exp.* **37** 47–63

[48] Huh D, Torisawa Y S, Hamilton G A, Kim H J and Ingber D E 2012 Microengineered physiological biomimicry: organs-on-chips *Lab Chip* **12** 2156–64

[49] Torres Palomino D C and Marti L C 2015 Chemokines and Immunity *Einstein* **13** 469–73

[50] Neumann E, Lefèvre S, Zimmermann B, Gay S and Müller-Ladner U 2010 Rheumatoid arthritis progression mediated by activated synovial fibroblasts *Trends Mol. Med.* **16** 458–68

[51] Jang S, Kwon E-J and Lee J J 2022 Rheumatoid arthritis: pathogenic roles of diverse immune cells *Int. J. Mol. Sci.* **23** 905

[52] Occhetta P, Mainardi A, Votta E, Vallmajo-Martin Q, Ehrbar M, Martin I, Barbero A and Rasponi M 2019 Hyperphysiological compression of articular cartilage induces an osteoarthritic phenotype in a cartilage-on-a-chip model *Nat. Biomed. Eng.* **3** 545–57

[53] Mondadori C, Visone R, Rasponi M, Redaelli A, Moretti M and Lopa S 2018 Development of an organotypic microfluidic model to reproduce monocyte extravasation process in the osteoarthritic joint *Osteoarthr. Cartil.* **26** S122